

Chapter 7

A Weak Signal Detection Method Based on Stochastic Resonances and Its Application to the Fault Diagnosis of Critical Mechanical Components

Niaoqing Hu, Bin Fan, Lei Hu, Zhe Cheng, Lun Zhang,
Guoying Zhao and Fengshou Gu

Abstract This chapter presents studies on the enhanced detection of characteristic signals from critical mechanical components such as bearings by the nonlinear effect of stochastic resonance (SR). In the past decades, classical stochastic resonance (CSR) method has been extensively studied to enhance the fault detection of these critical mechanical components such as bearings and gears. Based on CSR theories, the main content of this chapter includes two parts. The first is aiming at identifying the component characteristic frequencies in the spectra, SR normalized scale transform is proposed based on parameter-tuning bistable SR model, which leading to a new method via averaged stochastic resonance (ASR) to enhance the result of incipient fault detection. Then, rather than achieving the improvement of the signal-to-noise ratio (SNR) by increasing the noise intensity, a new approach is developed based on adding a harmonic excitation with a frequency based on the system's Melnikov scale factor to the system while the noise is left unchanged. The effectiveness of this method is confirmed and replicated by numerical simulations. Combined with the strategy of the scale transform, the method can be used to detect weak periodic signal with arbitrary frequency buried in the heavy noise. In addition, the chapter also presents the case study of applying these methods for the enhancement of fault characteristic signals in detecting incipient faults of roller bearings.

N. Hu (✉) · B. Fan · L. Hu · Z. Cheng · L. Zhang · G. Zhao
Key Laboratory of Science and Technology on Integrated Logistics Support, School of
Mechatronics Engineering and Automation, National University of Defense Technology,
Changsha 410073, Hunan, People's Republic of China
e-mail: hnq@nudt.edu.cn

F. Gu
Centre for Diagnostic Engineering, University of Huddersfield, Huddersfield, Yorkshire, UK

7.1 Introduction

Fault detection of critical mechanical components, such as bearings and gears of a power train in complex machines like helicopters and wind turbines, is one of the important tasks in the field of running reliability. It is well known that the evaluation of the dynamic behavior of the mechanical components solely depends on the quality of the measured signals. The factors such as the influence of their transmission path, the transmission medium, the ambient environment, change of internal dynamics etc., degrade the measured signals, leading to measurements with low signal-to-noise ratio (SNR). In many cases, the useful information is buried in the noise seriously so that it can be hardly recovered by conventional method. It means that the early signatures of possible potential faults may be missed, which would lose the chance to prevent the catastrophic failures induced by the mechanical components like helicopters. Thus, the detection issue of early symptoms of a dynamic mechanical component fault is essentially a topic of weak signal detection.

Therefore, weak signal detection under heavy background noise becomes more and more important for early detection of fault. Over the last decades, it is commonly concerned by scientists and engineers to detect and enhance weak target signal more expeditiously and precisely in noise environment with special restrictions. Therefore, some notions concerning weak signal detection were recommended. Several approaches have been applied to weak signal detection, such as chaotic resonator [1, 2], difference resonator [3], wavelet analysis [4], holospectral analysis, high order statistics, Hilbert-Huang transform and so on [5]. Furthermore, an enhanced detection solution for weak signals based on stochastic resonance theory has been presented, which can detect a weak signal in the presence of heavy noise from a very short data record [6].

In this chapter, two new enhanced detection approaches are presented based on extended stochastic resonance theory to detect weak signal in the presence of heavy noise. One is ‘averaged’ enhanced detection strategy based on normalized scale stochastic resonance model [5] to detect weak signal. The other effective SNR enhancement is achieved by adding a harmonic excitation with frequency based on the system’s Melnikov scale factor to the system while the noise is left unchanged.

Although the principle and property have been illustrated previously [7–9], key issues deeply related to SR and its application in weak mechanical signal processing will be discussed. Through a kind of normalized scale transform, the frequency range of weak signal SR model can detect is extended from low frequency to relative higher frequency. Based on normalized scale transform, a new method via averaged stochastic resonance (ASR) is presented to enhance the result of rolling element bearing fault detection furtherly.

Furthermore, in classical SR, the SNR can be improved by increasing the noise. But the approach by increasing the noise is counterintuitive and unwieldy. According to Melnikov theory, for a wide class of systems, deterministic and stochastic excitations play qualitatively equivalent roles in inducing chaotic

motions with escapes over a potential barrier [10]. Such motions therefore possess common qualitative features that suggest the extension of SR approaches beyond classical SR, so that the SNR can alternatively be improved by keeping the noise unchanged and adding a deterministic excitation which is close to the detected signal and selected in accordance with Melnikov theory, rather than by increasing the noise.

7.2 Fundamental of SR and Normalized Scale Transform

7.2.1 Fundamental of SR

The study of stochastic resonance in signal processing has received considerable attention over the last decades. In the context, stochastic resonance is commonly used as an approach to increase the SNR at the output through the increase of the special noise level at input signal. For a class of multistable system with noise and a periodic signal, the improvement of SNR achieved by increasing the noise intensity is known as stochastic resonance (SR) which will be referred to classical SR. The essence of the physical mechanism underlying classical SR has been described in [5–9]. Considering the motion in a bistable double-well potential of a lightly damped particle subjected to stochastic excitation and a harmonic excitation (i.e., a signal) with low frequency ω_0 . The signal is assumed to have small amplitude that, by itself (i.e., in the absence of the stochastic excitation), it is unable to move the particle from one well to another. It is denoted that the characteristic rate, that is, the escape rate from a well under the combined effects of the periodic excitation and the noise, by $\alpha = 2\pi n_{tot}/T_{tot}$, where n_{tot} is the total number of exits from one well during time T_{tot} . The behavior of the system will change when increasing the noise while the signal amplitude and frequency are unchanged. For zero noise, $\alpha = 0$, as noted earlier. For very small noise, $\alpha < \omega_0$. However, as the noise increases gradually, the ordinate of the spectral density of the output noise at the frequency ω_0 , denoted by $\Phi_n(\omega_0)$, and the characteristic rate α increases accordingly. Experimental and analytical studies show that, until $\alpha \approx \omega_0$, a cooperative effect (i.e., a synchronization-like phenomenon) occurs wherein the signal output power $\Phi_s(\omega_0)$ increases as the noise intensity increases. Remarkably, the increase of $\Phi_s(\omega_0)$ with noise is faster than that of $\Phi_n(\omega_0)$. This results in an enhancement of the SNR. The synchronization-like phenomenon plays a key role in the mechanism as described in [10].

At present, the most common studied SR system is a bistable system, which can be described by the following Langevin equation

$$\dot{x} = ax - bx^3 + A \sin(\omega_0 t + \phi_0) + \Gamma(t) \quad (7.1)$$

where $\Gamma(t)$ is noise term and $\langle \Gamma(t), \Gamma(0) \rangle = 2D\delta(t)$, $A \sin(\omega_0 t + \phi_0)$ is a periodic driving signal. Generally, it is also written as the form of Duffing equation

$$\ddot{x} = -\beta\dot{x} + ax - bx^3 + A \sin(\omega_0 t + \phi_0) + \Gamma(t) \quad (7.2)$$

where β is the damping coefficient.

7.2.2 Normalized Scale Transform of SR Model

Equation (7.1) has two stable solutions $x_s = \pm\sqrt{a/b} = \pm c$ (stable points) and an unstable solution $x_u = 0$ (unstable point) when $A = D = 0$, here the potential of Eq. (7.1) is given by

$$V(x) = -\frac{1}{2}ax^2 + \frac{1}{4}bx^4 \quad (7.3)$$

The height of potential is

$$\Delta V = V(0) - V(c) = \frac{a^2}{4b} \quad (7.4)$$

When adding the modulation signal, potential function is

$$V(x, t) = -\frac{1}{2}ax^2 + \frac{1}{4}bx^4 - Ax \cos \omega_0 t \quad (7.5)$$

For a stationary potential, and for $D \ll \Delta V$, the probability that a switching event will occur in unit time, i.e. the switching rate, is given by the Kramers formula [11]

$$r_0 = (2\pi)^{-1} [V''(0)|V''(c)]^{1/2} \exp(-\Delta V/D) \quad (7.6)$$

where $V''(x) \equiv d^2V/dx^2$. When a periodic modulation term $A \sin \omega_0 t$ is included on the right-hand-side of Eq. (7.1), it leads to a modulation of the potential Eq. (7.5) with time and an additional term $-Ax \cos \omega_0 t$ is now present on the right-hand-side of Eq. (7.5). In this case, the Kramers rate Eq. (7.6) becomes time-dependent:

$$r(t) \approx r(0) \exp(-Ax \sin \omega_0 t/D) \quad (7.7)$$

Which is accurate only for $A \ll \Delta V$ and $\omega_0 \ll \{V''(\pm c)\}^{1/2}$. The latter condition is referred to as the adiabatic approximation. It ensures that the probability density corresponding to the time-modulated potential is approximately stationary (the modulation is slow enough that the instantaneous probability density can ‘adiabatically’ relax to a succession of quasi-stationary states). The slow modulation means that the signal to detect is confined to a rather low frequency range and small amplitude. It is well known that the characteristic frequency reflecting mechanical

system state exceeds the range of limit, so how to detect the high frequency signal is of great importance in weak characteristic signal detection of mechanical system.

To overcome the low frequency limitation of SR, a scale transform needs to be introduced to shift the frequency of interest into the range in which SR operates. Considering the bistable system modeled by Eq. (7.1), where A is the amplitude of the input signal, $\omega \gg 1$ is its frequency, $\Gamma(t)$ is Gaussian white noise with the correlation $\langle \Gamma(t) \rangle = 0$; $\langle \Gamma(t), \Gamma(0) \rangle = 2D\delta(t)$, and D is the noise intensity, when a and b are positive real numbers, a variable substitution can be carried out by

$$z = x\sqrt{b/a}, \quad \tau = at \quad (7.8)$$

Substituting Eq. (7.8) into Eq. (7.1) yields:

$$a\sqrt{\frac{a}{b}}\frac{dz}{dt} = a\sqrt{\frac{a}{b}}z - a\sqrt{\frac{a}{b}}z^3 + A\cos\left(\frac{\omega_0}{a}\tau + \phi_0\right) + \Gamma\left(\frac{\tau}{a}\right) \quad (7.9)$$

where the noise $\Gamma(\tau/a)$ satisfies $\langle \Gamma(\tau/a)\Gamma(0) \rangle = 2Da\delta(\tau)$. Therefore

$$\Gamma\left(\frac{\tau}{a}\right) = \sqrt{2Da}\xi(\tau) \quad (7.10)$$

where $\langle \xi(\tau) \rangle = 0$, $\langle \xi(\tau), \xi(0) \rangle = \delta(\tau)$.

Substituting Eq. (7.10) into Eq. (7.9) results in:

$$a\sqrt{\frac{a}{b}}\frac{dz}{dt} = a\sqrt{\frac{a}{b}}z - a\sqrt{\frac{a}{b}}z^3 + A\cos\left(\frac{\omega_0}{a}\tau + \phi_0\right) + \sqrt{2Da}\xi(\tau) \quad (7.11)$$

Equation (7.11) can be simplified into

$$\frac{dz}{dt} = z - z^3 + \sqrt{\frac{b}{a^3}}A\cos\left(\frac{\omega_0}{a}\tau + \phi_0\right) + \sqrt{\frac{2Db}{a^2}}\xi(\tau) \quad (7.12)$$

Equation (7.12) is a normalized form and equals to Eq. (7.1). The frequency of the signal after the scale transform is $1/a$ times of which before transform. Hence, through the chosen of larger parameter a , a high frequency signal can be normalized to lower one to satisfy the request of the theory of SR.

During the numerical simulation, the variance σ^2 is used to describe the statistical property of the white noise. As the noise intensity D is influenced by sample step h , the actual value $D = \sigma^2 h/2$. If RMS value of the noise is $\sigma_0 = \sqrt{2D/h}$ before transform, the intensity of the noise will change to $2Db/a^2$ after the transform. In addition, because the sample frequency descends, the sample step becomes a times of the original sample step. Therefore, the RMS of the noise after transform is $\sigma = \sqrt{2Db/(a^2 \cdot ah)}$. The ratio of the noise RMS after the transform to which before the transform is

$$\sigma/\sigma_0 = \sqrt{b/a^3} \quad (7.13)$$

It is easy to be seen that, after the transform, the signal and noise are amplified $\sqrt{b/a^3}$ times.

7.2.3 Averaged SR Model with Normalized Scale Transform

Taking $y(t)$ as the sampled signal or the envelop signal of raw signal with Hilbert transform (as described in Sect. 4.1), Eq. (7.12) can be written as

$$\frac{dz}{d\tau} = z - z^3 + \sqrt{\frac{b}{a^3}}y(\tau) + \sqrt{\frac{2Db}{a^2}}\xi(\tau) \quad (7.14)$$

Then Eq. (7.14) can be solved numerically J times with different $\xi_i(\tau)$ ($i = 1, 2, \dots, J$) to obtain $z_i(\tau)$ ($i = 1, 2, \dots, J$), then an average is carried out by

$$\bar{z}(\tau) = \frac{1}{J} \sum_{i=1}^J z_i(\tau) \quad (7.15)$$

Through this average procedure a more reliable detection result can be obtained, which is a general operation based on the Mont Carlo principle.

7.2.4 Model Validation Using Simulated Data

To evaluate the performance of the scale transform proposed a numerical simulation study is carried out based on a mixed signal to be enhanced through the model of bistable system with parameters $a = b = 1$, $A = 0.5$, $f = 0.1$ Hz, $\sigma = 5$, $f_s = 20$ Hz, $N = 2,000$.

Figure 7.1a, b shows the mixed signal and its spectrum, while Fig. 7.1c, d gives the output of the bistable system and the spectrum of the output signal. From Fig. 7.1d, it can be seen that although the input $\text{SNR} = 20 \log(A/\sigma) = -20$ dB, there is a clear spectrum line at $f = 0.1$ Hz, and the noise attenuation is obvious.

If the signal frequency is changed into $f = 1$ kHz, according to the transform principle, the parameters $a = b = 10^4$, $f_s = 200$ kHz and $N = 2,000$ can be used for frequency shift. The mixed signal will be amplified by $\sqrt{a^3/b} = 10,000$ times. Applying SR enhancement to this mixed signal after the transform produces results as shown in Fig. 7.2.

As it can be seen in Fig. 7.2, the signal and spectrum is consistent with that of Fig. 7.1 although they show differences in the scales the time domains and frequency coordinates. The noise components are greatly suppressed, and the

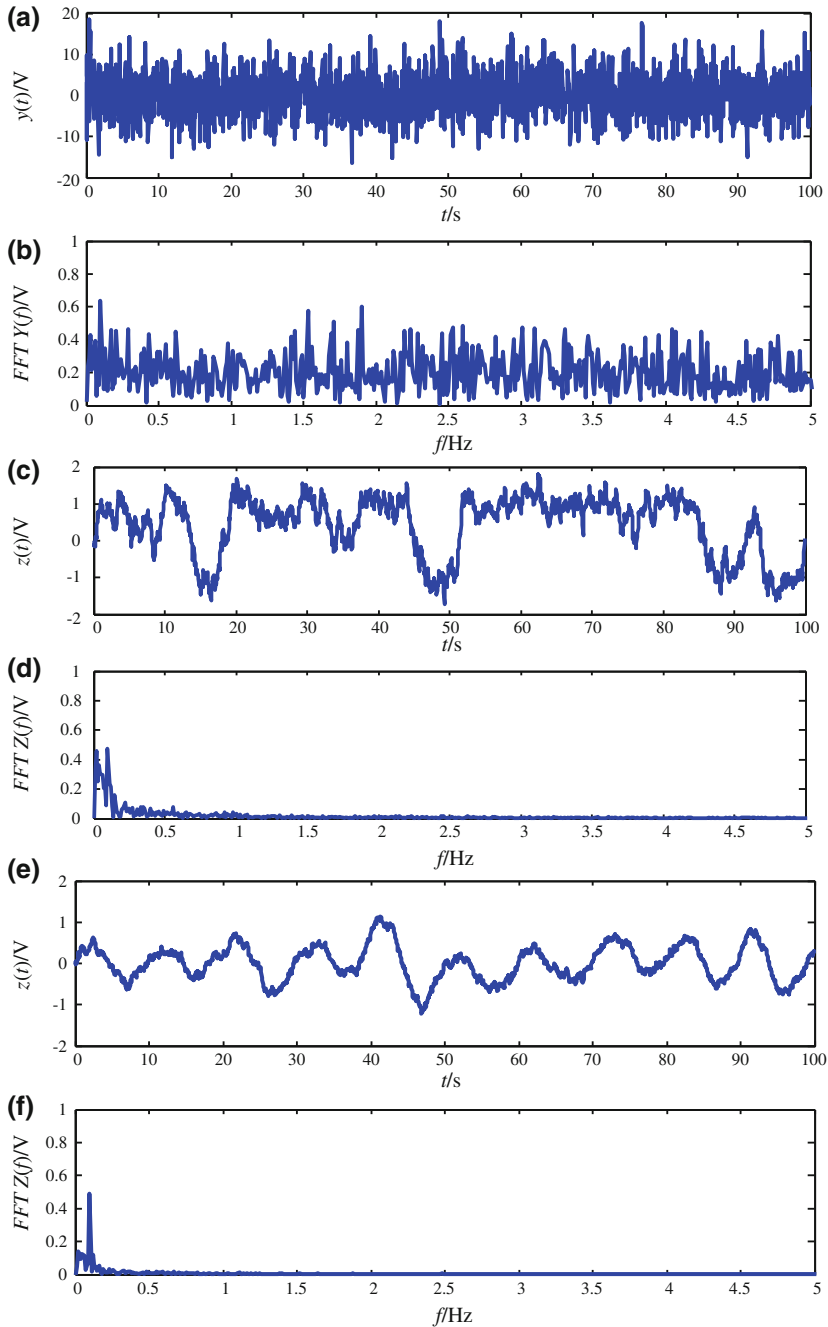


Fig. 7.1 Time-domain and its FFT of the input and output when $f = 0.1$ Hz. **a** and **b** the input; **c** and **d** the output by one-time; **e** and **f** the output by averaged

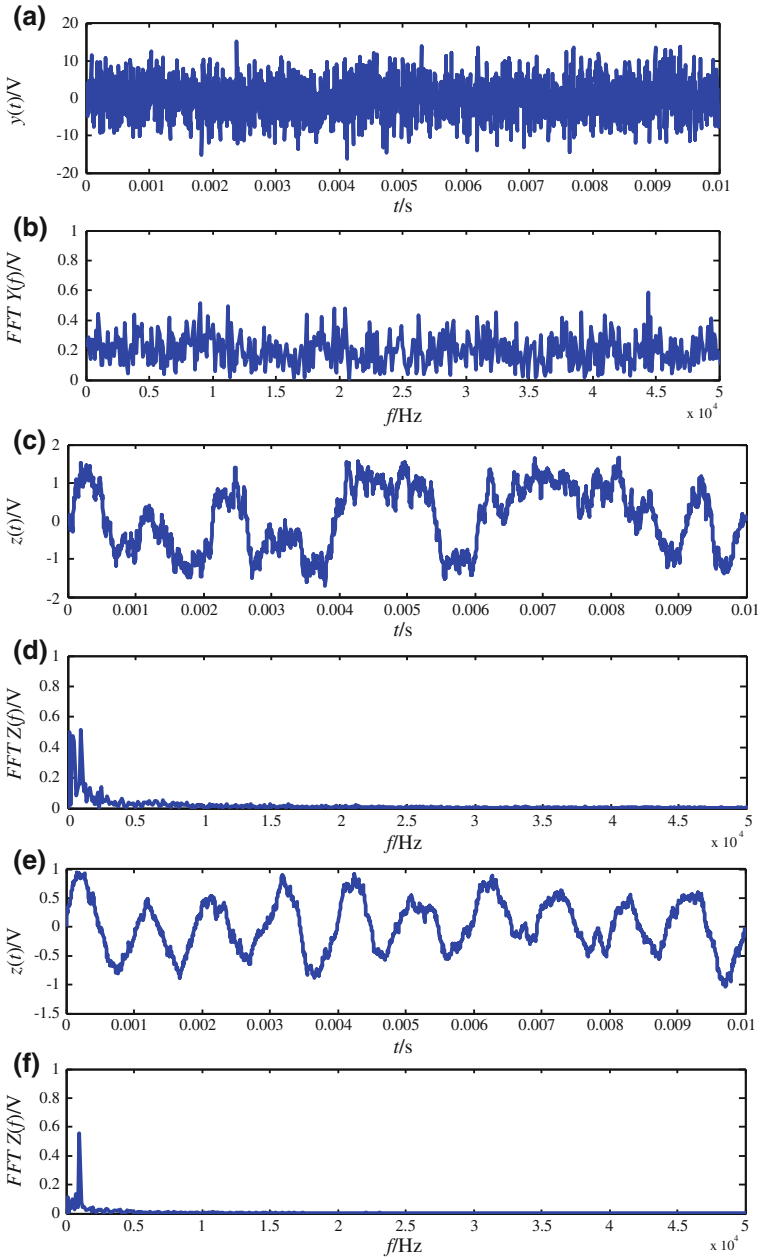


Fig. 7.2 Time-domain and its FFT of the input and output when $f = 1$ kHz. **a** and **b** the input; **c** and **d** the output by one-time; **e** and **f** the output by averaged

detecting signal is standing out, which shows that the transform method is effective for adapting to the behavior of SR to enhance high frequency signals. Therefore, by adjusting parameter a of the bistable system, SR model can adapt to different frequency signal, while by adjusting parameter b , it can adapt to different noise intensity. In addition, compared (d) with (f) of Figs. 7.1 and 7.2, it is obvious that the averaged SR results are better than that of one-time SR result.

7.3 SR Model by Adding a Harmonic Excitation

7.3.1 SR Interpretation via Melnikov Theory and Chaotic Dynamic Approach

As stated in [10, 11], for a bistable system with noise and a periodic signal, the improvement of the signal-to-noise ratio (SNR) achieved by increasing the noise intensity is known as stochastic resonance (SR) (i.e., classical SR in these papers). Here, the signal to noise ratio (SNR) is expressed in dB as $SNR = 10\log_{10}(S/N)$, where S and N are, respectively, the ordinate of the output power spectrum and the ordinate of the broadband output power spectrum at the signal frequency ω_0 . As described in Sect. 2.1, the synchronization like phenomenon plays a key role in the SR mechanism.

Now we consider second-order dynamical systems described by the following equation [10]

$$\ddot{x}(t) = -\beta\dot{x}(t) - V'(x) + G(t) \quad (7.16)$$

where $V(x)$ is a potential function. The unperturbed counterpart of Eq. (7.1) is the Hamiltonian system expressed by $\ddot{x} = -V'(x)$. We assume that $V(x)$ is a double-well potential (Duffing-Holmes) as described in (7.3) with $a = b = 1$. $\ddot{x} = -V'(x)$ with the potential (7.3) and $a = b = 1$ has the homoclinic orbits [12].

Firstly, it is assumed that the excitation is only periodic, that is, in Eq. (7.16) $G(t) \equiv A_0 \sin(\omega_0 t)$. According to the Smale-Birkhoff theorem, the necessary condition for the occurrence of chaos is that the Melnikov function induced by the perturbation has simple zeroes. For Duffing system this condition is the Melnikov inequality

$$-(4/3)\beta + A_0 S_M(\omega_0) > 0 \quad (7.17)$$

where

$$S_M(\omega) = \sqrt{2}\pi\omega \operatorname{sech}(\pi\omega/2) \quad (7.18)$$

is a system property known as the Melnikov scale factor [13].

Secondly, assume that the excitation consists of the quasiperiodic sum

$$G(t) \equiv A_0 \sin(\omega_0 t + \phi_0) + A_a \sin(\omega_a t) + \sum_{k=1}^K a_k \sin(\omega_k t + \phi_k) \quad (7.19)$$

For this case a generalization of the Smale-Birkhoff theorem [13] yields the Melnikov inequality as the necessary condition for chaos

$$-\frac{4\beta}{3} + A_0 S_M(\omega_0) + A_a S_M(\omega_a) + \sum_{k=1}^K a_k S_M(\omega_k) > 0 \quad (7.20)$$

Finally, assume that the system's excitation is

$$G(t) \equiv A_0 \sin(\omega_0 t + \phi_0) + A_a \sin(\omega_a t) + \sqrt{2D\beta}R(t) \quad (7.21)$$

where $R(t)$ is a Gaussian process with unit variance and spectral density $g(\omega)$. Over any finite time interval, however large, each realization of the process $R(t)$ may be approximated as closely as desired by a sum [10]

$$R_N(t) = \sum_{k=1}^K b_k \sin(\omega_k t + \phi_k) \quad (7.22)$$

so that the Melnikov inequality, that is, the necessary condition for chaos, can be written as in Eq. (7.20) where $a_k = \sqrt{2D\beta}b_k$. In formula (7.22), $b_k = \sqrt{g(\omega_k)\Delta\omega}$, ϕ_k are randomly chosen phases of uniform distribution on the interval $[0, 2\pi]$ and $\omega_k = k\Delta\omega$, $\Delta\omega = \omega_{\max}/K$, ω_{\max} is the frequency beyond which the spectrum vanishes (the cutoff frequency).

For the damped, forced system, the existence in a plane of section of a transverse point of intersection between the stable and unstable manifolds implies the existence of infinity of intersection points. Eventually, they may form a chaotic motion under a particular excitation. The strength of the chaotic transport, and therefore the characteristic rate α , increases as the left-hand side of in Eq. (7.20) becomes larger [13]. This is true regardless of whether the excitation is deterministic or stochastic. Moreover, again regardless of whether the excitation is deterministic or stochastic, a qualitative feature of the chaotic motions featuring escapes is that their spectral densities have a broadband portion with significant energy content at and near the system's characteristic rate α . Thus, we expect that we can build a bridge between chaos and stochastic resonance. That is to say, we can explain SR phenomena by chaotic dynamics approach.

Assume that the excitation is a sum of a harmonic signal and an additional harmonic component, that is, in Eq. (7.16), $G(t) \equiv A_0 \sin(\omega_0 t) + A_a \sin(\omega_a t)$. The system is therefore deterministic with, in general, quasiperiodic excitation. The necessary condition for chaos is given by in Eq. (7.20) in which $a_1 = a_2 = \dots = a_K = 0$. We choose A_0 so that, for $A_a = 0$, the motion is confined

to one well. In accordance with Melnikov theory this will be the case if the Melnikov inequality given by in Eq. (7.17) is not satisfied. We now add the excitation $A_a \sin(\omega_a t)$. For a certain region R_a of the parameter space $[A_a, \omega_a]$, the system can experience chaotic motion with jumps over the potential barrier. The Melnikov scale factor $S_M(\omega)$ provides the information needed to select frequencies ω_a such that the added excitation is effective in inducing chaotic behaviour. In general, ω_a should be equal or close to the frequency for which $S_M(\omega)$ is the largest.

Given the existence in the spectrum of a broadband portion qualitatively similar to that present in the case of classical SR, it is reasonable to expect that the synchronization like phenomenon that occurs in the classical SR case would similarly occur for the deterministically excited chaotic system. This was verified by a numerical simulation for a large number of cases. As a typical example in [10], the case for $\beta = 0.316$, $A_0 = 0.095$, $\omega_0 = 0.0632$ (for these values in Eq. (7.17) is not satisfied) and $\omega_a = 1.1$ is examined. Spectral densities of motions with these parameters and $A_a = 0.263$, 0.287 , and 0.332 , are shown in (a), (b) and (c) of Fig. 7.3, respectively. As it can be seen in Fig. 7.3a, when $\alpha = 0.0671$ is close to the signal frequency $\omega_0 = 0.0632$, The energy in the broadband portion of the spectrum is reduced clearly, while the energy at the signal's frequency is enhanced, compared with the respective counterparts in Fig. 7.3b, c, for which $\alpha = 0.0518$ and $\alpha = 0.1611$, respectively. The synchronization like phenomenon noted for classical SR is thus clearly evident in Fig. 7.3b. In addition, the motions in Fig. 7.3 of (a), (b), (c) are indeed chaotic. This shows that the additive harmonic signal plays the same effect as the noise in the enhancement of SNR.

7.3.2 Simulation for Enhancing the Detection of Weak Signal by Adding a Harmonic Excitation

7.3.2.1 Detecting Weak Signal at Low Frequency

Notice that the larger the left-hand side of Eq. (7.20), the stronger is the chaotic transport, and therefore the larger is the rate α . Let $A_a = 0$, $a_k = \sqrt{2D\beta} \sqrt{g(\omega_k) \Delta\omega}$ in Eq. (7.20). It is therefore clear from in Eq. (7.20) that for any given power of the stochastic excitation $2D\beta$, the left-hand side of Eq. (7.20) becomes larger and the rate α increases. We thus obtain the interesting qualitative result that, for a given Melnikov scale factor $S_M(\omega)$ and a given power of the stochastic excitation, the rate α increases as the spectral power of the excitation is distributed nearer to the frequency of $S_M(\omega)$'s peak, ω_{pk} (the greatest effectiveness being achieved by a single component with frequency equal or close to ω_{pk}).

We now illustrate the usefulness of this result for a system with classical SR (i.e., one for which in Eq. (7.21) $A_a = 0$, $D > 0$). We assume $R(t)$ has the Lorentzian spectral distribution $g(\omega) = \gamma(1 + \omega^2\tau^2)^{-1}$ cut off at the frequency ω_{max} ; τ is the correlation time and γ is a normalization constant such that the variance of $R(t)$ is

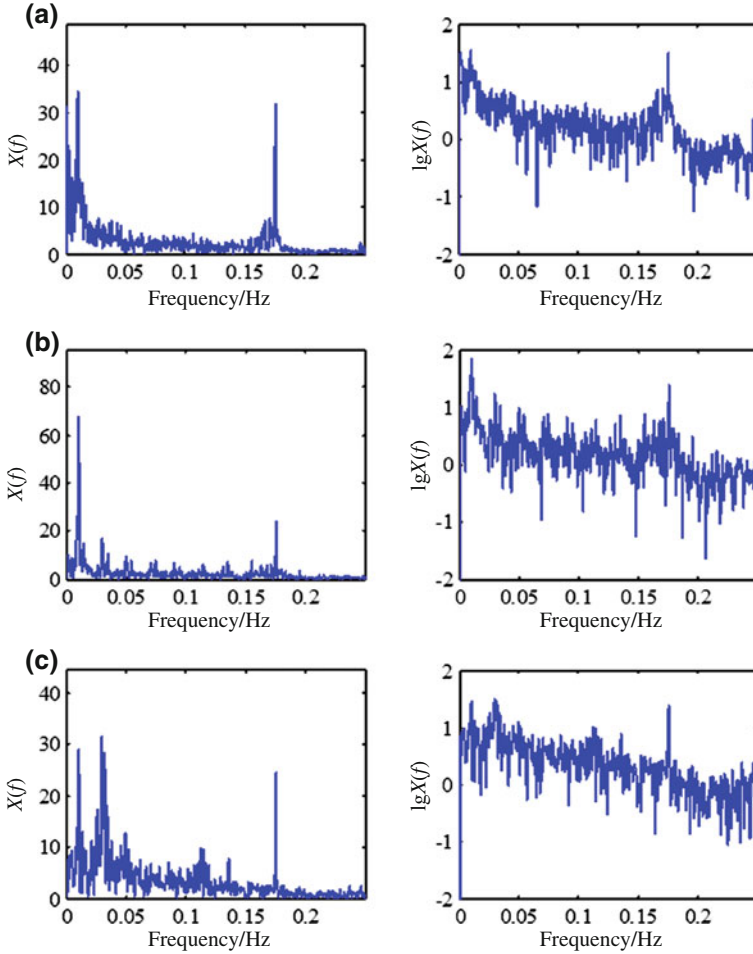


Fig. 7.3 Amplitude spectra of system with $D = 0$, A_0 and ω_0 keep constant. **a** The system is subjected to an additional harmonic excitation with $\omega_a = 1.1$ and $A_a = 0.263$. **b** All settings are the same as in, **a** except amplitude $A_a = 0.287$. **c** All settings are the same as in, **a** except amplitude $A_a = 0.332$

unity. The Melnikov scale factor $S_M(\omega)$ would in practice suppress contributions of components with frequencies $\omega > \omega_{\max}$.

Considering the case $\tau = \tau_1 = 0.2$, typical averaged output spectra $P(\omega)$ for $A_0 = 0.3$, $\omega_0 = 0.069$, $\omega_{\max} = 3.0$, $\beta = 0.25$ are shown in Fig. 7.4a–c for $D = 0.1$, 0.6, and 2.0, respectively (other parameters are the same as in [10]). The averaging was performed over 225 noise realizations approximated by in Eq. (7.20) with $100 < K < 500$. Note that $A_0 < 4\beta/3S_M(\omega_0)$, so that no chaotic behaviour can be induced by the periodic signal alone. However, it was verified that, for the noise realizations used to obtain the results of Fig. 7.4a–c, the Melnikov inequality given

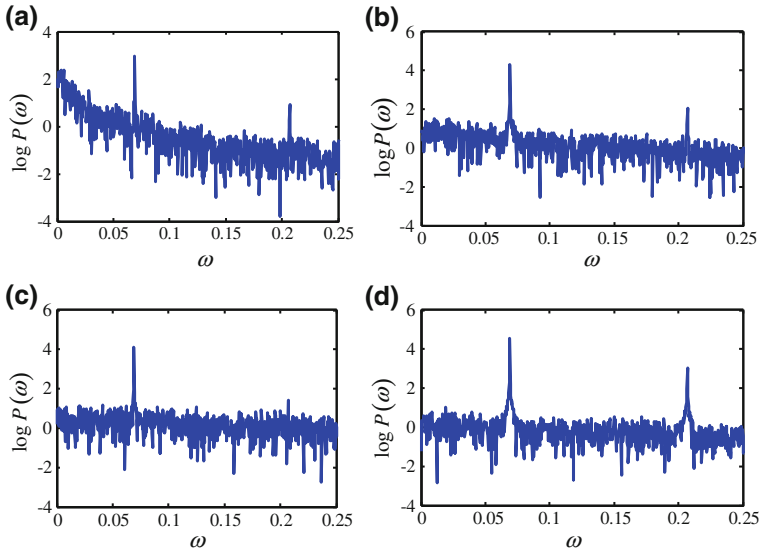


Fig. 7.4 Averaged power spectra of output for stochastically excited system: **a–c** increasing noise intensity D and $A_a = 0$. **d** The same noise intensity D as in **a**, and $A_a = 0.23$. Noise correlation time $\tau = 0.2$

by in Eq. (7.20) was satisfied, and that the respective motions were chaotic. Energy transfer to the signal frequency was found to be the highest when the rate α for the chaotic motion is close to the signal frequency ($\alpha = 0.0077$, $\alpha = 0.0667$, $\alpha = 0.1772$ for Fig. 7.4a–c, respectively).

As illustrated earlier, assume that $A_a = 0$, and that for a set of values A_0 , ω_0 , β and D the system has low SNR. We could improve the SNR by increasing D . However, it is more effective to increase the SNR by keeping D unchanged and adding an excitation $A_a \sin(\omega_a t)$ such that ω_a is equal or close to the frequency of $S_M(\omega)$'s peak and A_a is so chosen as to bring about a characteristic rate comparable to the signal frequency. In Fig. 7.4d, all parameters and the normalized spectrum $g(\omega)$ are the same as for Fig. 7.4a, except that the system is subjected to an additive sinusoidal excitation with amplitude $A_a = 0.23$ and frequency $\omega_a = 1.1$. This approach to increasing SNR is seen to be effective by comparing Fig. 7.4d with b (in Fig. 7.4d, $\alpha = 0.0706$ close to ω_0).

7.3.2.2 Detecting Weak Signal with Arbitrary Frequency

From Eq. (7.18), we can get that $S_M(\omega)$ achieves the maximum when $\omega \approx 0.76$. Once the frequency ω_a of additive harmonic excitation is equal or close to the frequency of $S_M(\omega)$'s peak, the SNR improvement is obvious. That is to say, the frequency of the detected characteristic signal only satisfies $\omega \leq \omega_{\max} \approx 3.0$ and is

very low. Now the problem is how to detect weak signal with arbitrary frequency by the method discussed above?

Combining Eqs. (7.3) and (7.16) obtains

$$\ddot{x} = -\beta\dot{x} + x - x^3 + G(t) \quad (7.23)$$

where $G(t)$ is expressed by Eq. (7.21), In general, let the added harmonic $\omega_a = 1.0$ and detected signal $\omega_0 < \omega_a$. By assuming that $t = \omega_1\tau$, Eq. (7.23) becomes

$$\frac{1}{\omega_1^2} \frac{dx^2}{d\tau^2} = -\frac{\beta dx}{d\tau} + x - x^3 + G(\tau) \quad (7.24)$$

Let $x_1 = x$, $x_2 = \frac{1}{\omega_1} \frac{dx}{d\tau}$, rewrite Eq. (7.24) to be state equation

$$\begin{aligned} \frac{dx_1}{d\tau} &= \omega_1 x_2 \\ \frac{dx_2}{d\tau} &= \omega_1 (-\beta x_2 + x_1 - x_1^3 + G(\tau)) \end{aligned} \quad (7.25)$$

Thus, Eq. (7.25) can be applied to enhancement detection of weak characteristic signal with arbitrary frequency. It is important to emphasize that the normalized scale transform of SR described in Eq. (7.12) is used, instead of Eq. (7.25).

Now, as a typical example, assume that we want to detect a characteristic signal with amplitude $A_0 = 0.3$ and frequency $\omega_0 = 0.069 \times 2\pi \times 1,000$ (i.e., 69 Hz). In this case, $\omega_1 = 2\pi \times 1,000$, $\omega_a = 1.0 \times 2\pi \times 1,000$. Substituting these parameters into Eq. (7.25) obtains the solution as shown in Fig. 7.5. It can be seen that the SNR improvement is obvious from Fig. 7.6b.

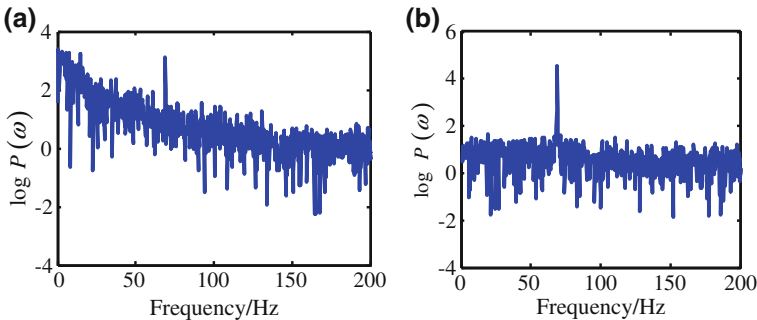


Fig. 7.5 Averaged power spectra of output for stochastically excited system: **a** increasing noise intensity $D = 0.1$ and $A_a = 0$ ($\alpha = 70.9466$, lower than $\omega_0 = 433.5398$ (i.e., 69 Hz)). **b** The same noise intensity D as in **a**, and $A_a = 0.23$, here $\alpha = 429.5146$ (i.e., 68.3594 Hz). Noise correlation time $\tau = 0.2$

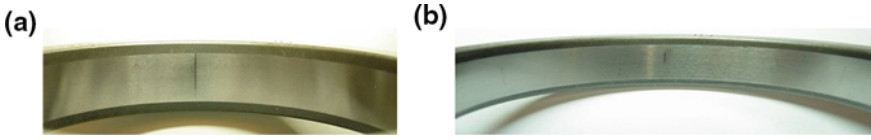


Fig. 7.6 Line defects seeded on the outer race of the test bearings. **a** MF ($0.3 \times 16 \text{ mm}^2$). **b** SF ($0.11 \times 6 \text{ mm}^2$)

7.4 Validation Using Experimental Data

The experimental data was from the Centre for Diagnostic Engineering at University of Huddersfield. The test rig consists of a three-phase electrical induction motor and a dynamic brake. The motor drives the brake by means of three shafts, which are joined by pairs of matched flexible couplings. The shafts are supported by two bearing housings, each containing one roller and one captive ball bearing. The bearing used in the experiments was a N406 roller bearing. The tested bearing was fitted in the bearing housing on the driven side.

In the experiments, the load applied to the test rig was 42.0 Nm and the rotational speed was 1,456 r/min (24.3 Hz). When the load was decreased, the rotational speed increased slightly. The three vibration signals were collected by accelerometers which were fixed on the cage near the tested bearings. Two different sizes of line defect were seeded on the outer race of bearings: a medium defect (approximately $0.3 \times 16 \text{ mm}^2$), shown in Fig. 7.6a; and a small defect (approximately $0.11 \times 6 \text{ mm}^2$), shown in Fig. 7.6b. Based on the geometric sizes and the rotational speed, the characteristic defect frequency (CDF) of the outer race was calculated to be 83.4 Hz. To get the finger print recordings, a defect free test was also conducted. All of the tests were repeated once during the experiments.

In the vibration data acquisition, the sampling rate was 64,938 Hz and the length of data was 810,439. For the convenience of analysis, the vertical radial acceleration signal was used to validate the SR-based algorithm for early detection of incipient fault. In the analysis, we extracted the data points by two times sampling interval. So the sampling rate was $f_s = 32,469 \text{ Hz}$. The length of data was selected to be $2^{17} = 131,072$.

7.4.1 Envelop Analysis

The amplitude envelope of the raw vibration signals is computed using an algorithm based on the Hilbert transform, H , which is defined by

$$H[s(t)] = \frac{1}{\pi} \int_{-\infty}^{\infty} s(\tau) \frac{1}{t - \tau} d\tau \quad (7.26)$$

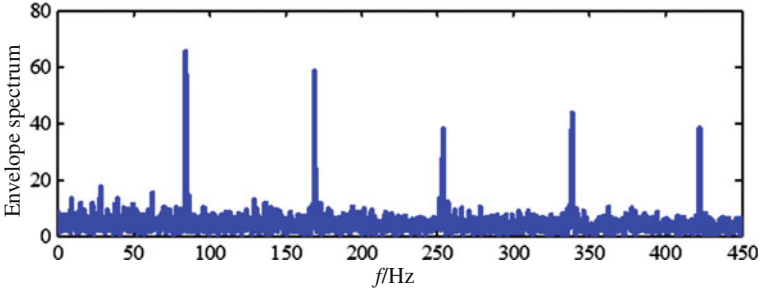


Fig. 7.7 A segment of FFT spectrum of envelope signal with medium defect

where $s(t)$ is a raw acceleration signal. Then the analytical signal, $\hat{s}(t)$, can be formed by

$$\hat{s}(t) = s(t) + jH[s(t)] \quad (7.27)$$

Thus the envelope of the raw acceleration signal can be computed by

$$En(t) = \sqrt{s^2(t) + H^2[s(t)]} \quad (7.28)$$

Finally, the signal computed by Eq. (7.28) is processed using the FFT to obtain the amplitude spectrum of the acceleration signal envelope. For the defect with certain degrees of severity, we can find that the component and its multiple components at the fault characteristic frequency are very obvious. For example, a classical result with medium defect of outer under middle load is shown in Fig. 7.7.

For the very small defect on the outer race, a classical results under the same load as that in medium defect are shown in Fig. 7.8. In this example, the selected pass band of filter is the same as that in medium defect. From Fig. 7.7, we can find that the signature frequency component and its multiple components are invisible and may be buried by the other unrelated components and random noise. That is to say, under the situation of incipient fault, the only envelope spectrum analysis cannot detect the small defect effectively and consistently.

7.4.2 SR Output of Driven by Envelope Signal

According to Eqs. (7.14) and (7.15) and the signature frequency component of outer defect, the benchmark frequency was selected to be $f = 60$ Hz for normalized scale transform of SR model. Some parameters are as follows. Added noise intensity $D = 0.0005$, $a = f/0.1 = 600$, $b = f/0.1 = 600$, model calculating time step $h = 1/f_s = 3.0799 \times 10^{-5}$, RMS of added noise $\sigma = \sqrt{2 \cdot D \cdot f_s} = 139.5752$.

The envelope signal of Fig. 7.7 plus added noise signal is considered to be the input signal and drives the model in Eq. (7.14). The corresponding results are shown in Fig. 7.9. Because the signature components in envelope spectrum are already obvious, the advantage of SR analysis cannot be exposed.

The envelope signal of Fig. 7.8 is considered to be the input signal and drives the model Eq. (7.14). The corresponding results are shown in Fig. 7.10. the signature

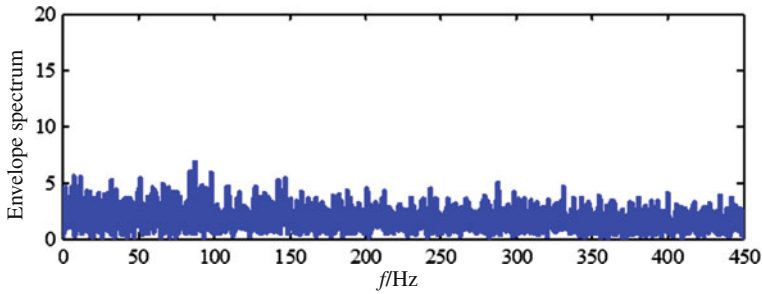


Fig. 7.8 A segment of FFT spectrum of envelope signal with small defect

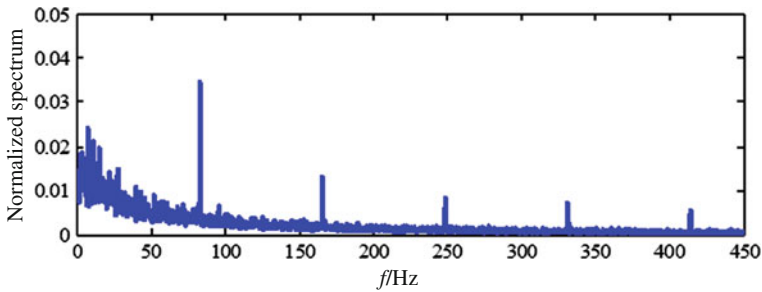


Fig. 7.9 The output results of SR model for vibration data of medium defect of outer

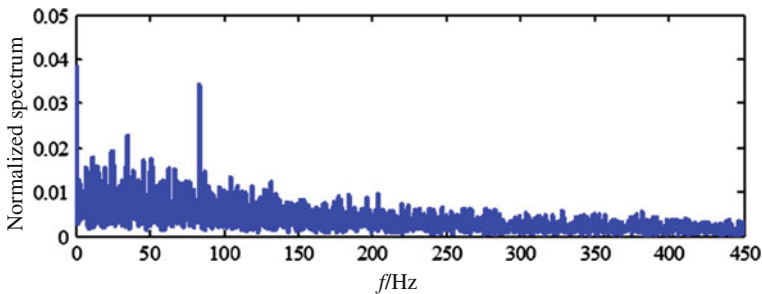


Fig. 7.10 The output results of SR model for vibration data of small defect of outer

component is very obvious in Fig. 7.10, in contrast, it is hard to be seen in the normal envelop spectrum in Fig. 7.8. This then clearly shows that SR is effective to enhance small signal component for incipient fault detection.

7.4.3 Weak Characteristic Signal Detection by SR of Adding a Harmonic Excitation

Based on the same data sets, the performance of the SR enhancement with adding harmonic excitation is examined. A segment of FFT spectrum of envelope signal analyzed from acceleration signal of small defect in outer race of bearings is shown in Fig. 7.11. The characteristic defect frequency of the outer race (about 83 Hz) cannot be found in Fig. 7.11. When the envelope signal with small defect and added harmonic signal drive the normalized scale transform of SR model in [12] or Eq. (7.25), respectively, results obtained are shown in Figs. 7.12 and 7.13 respectively. In these two figures, the characteristic defect frequency component of the outer race is relatively obvious (about 84 Hz), which shows that it is possible to use the approach of adding harmonic content for improving the performance of the SR based detection

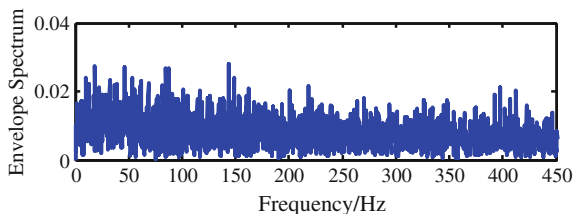


Fig. 7.11 A segment of FFT spectrum of envelope signal with small defect

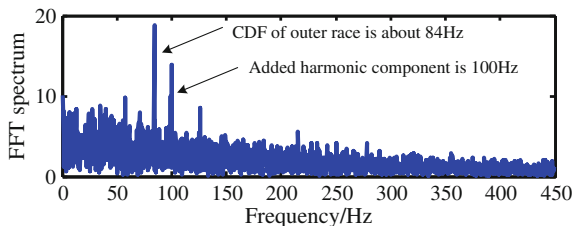


Fig. 7.12 A segment of FFT spectrum of output of scale transform of SR model in (7.12) was driven by envelope signal with small defect and added harmonic signal with $\omega_a = 2\pi \times 100$

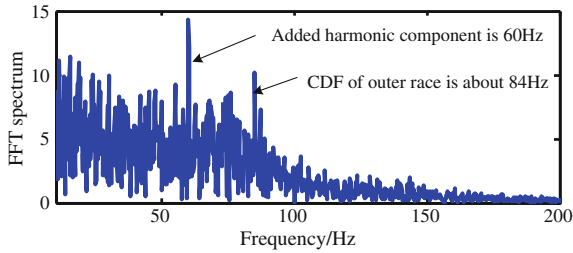


Fig. 7.13 A segment of FFT spectrum of output of Eq. (7.25) excited by envelope signal with small defect and added harmonic signal with $A_a = 0.07$ and $\omega_a = 2\pi \times 60$

7.5 Conclusion

According to the essence of classical stochastic resonance theory, the prominent role of the stochastic resonance phenomenon is that it can be used to boost weak signals embedded in a noisy environment. But for classical stochastic resonance, only weak signal with very low frequency can be detected in heavy noise. In this chapter, based on our recent studies [14–17], the signal enhancement via stochastic resonance is explained according to two main approaches. One is the scale transform of classical SR model for detecting relative higher frequency signal, thus the enhanced detection of periodic weak signal can be obtained via averaged approach. Another work is the investigation of the alternative mechanism for enhancing SNR, wherein the noise intensity is left unchanged but a harmonic excitation is added instead. This mechanism is shown more effective, allowing a better SNR to be obtained than the mechanism that of increasing the noise intensity. In addition, corresponding numerical simulations and case studies show that the proposed method for enhancing SNR is of more effectiveness.

Acknowledgments The authors would like to acknowledge the support of National Natural Science Foundation of China (Grant Nos. 51075391, 51105366, 51205401 and 51375484) and the Specialized Research Fund for the Doctoral Program of Higher Education of China under Grant No. 20114307110017.

References

1. Donald LB (1992) Chaotic oscillators and CMFFNS for signal detection in noise environment. *IEEE Int Jt Conf Neural Netw* 2:881–888
2. Hu NQ, Wen XS (2003) The application of duffing oscillator in characteristic signal detection of early fault. *J Sound Vib* 268(5):917–931
3. Qu LS, Lin J (1999) A difference resonator for detecting weak signals. *J Measur* 26(1):69–77
4. He ZJ et al (1996) Wavelet transform in tandem with autoregressive technique for monitoring and diagnosis of machinery. *Chin J Mech Eng (Engl Ed)* 9(4):311–317

5. Zhang XF, Hu NQ, Hu L, Cheng Z (2013) Multi-scale bistable stochastic resonance array: a novel weak signal detection method and application in machine fault diagnosis. *Sci China Technol Sci* 56(9):2115–2123
6. Hu NQ, Min C, Wen XS (2003) The application of stochastic resonance theory for early detecting rub-impact fault of rotor system. *Mech Syst Signal Process* 17(4):883–895
7. Benzi R, Sutera A, Vulpiani A (1981) The mechanism of stochastic resonance. *J Phys A: Math Gen* 14(11):453–457
8. De-chun G, Gang H, Xiao-dong W et al (1992) Experimental study of signal-to-noise ratio of stochastic resonance systems. *Phys Rev A* 46(6):3243–3249
9. Gammaitoni L (1998) Stochastic resonance. *Rev Mod Phys* 70(1):223–287
10. Franaszek M, Simiu E (1996) Stochastic resonance: a chaotic dynamics approach. *Phys Rev E* 54(2):1298–1304
11. McNamara B, Wiesenfeld K (1989) Theory of stochastic resonance. *Phys Rev A* 39(9):4854–4869
12. Guckenheimer J, Holmes P (1990) *Nonlinear oscillations, dynamical systems, and bifurcations of vector fields*. Springer, New York
13. Wiggins S (1992) *Chaotic transport in dynamical systems*. Springer, New York
14. Zhang XF, Hu NQ, Cheng Z et al (2012) Enhanced detection of rolling element bearing fault based on stochastic resonance. *Chin J Mech Eng* 25(6):1287–1297
15. Zhang XF, Hu NQ, Hu L et al (2013) Stochastic resonance in multi-scale bistable array. *Phys Lett A* 377:981–984
16. Zhang XF, Hu NQ, Hu L et al (2012) Enhanced detection of bearing faults based on signal cepstrum pre-whitening and stochastic resonance (in Chinese). *J Mech Eng* 48(23):83–89
17. Hu N, Hu L, Zhang X, Gu F, Ball A (2012) Enhancement detection of characteristic signal using stochastic resonance by adding a harmonic excitation. In: *The 25th international congress on condition monitoring and diagnostic engineering management (COMADEM2012)*, 17th–20th June 2012. Electronic application, Huddersfield, UK pp 34–43